JOURNAL OF SYNCHROTRON RADIATION
ISSN 1600-5775

Refurbishment of a used in-vacuum undulator from the National Synchrotron Light Source for the National Synchrotron Light Source-II ring

Toshiya Tanabe,[a]* Harmanpreet Bassan,[a] Andrew Broadbent,[a] Peter Cappadoro,[a] John Escallier,[a] David Harder,[a] Charles Hetzel,[a] Dean Hidas,[a] Charles Kitegi,[a] Bernard Kosciuk,[a] Marco Musardo[a] and Johnny Kirkland[b]

[a]National Synchrotron Light Source-II, Brookhaven National Laboratory, Bldg 744, Upton, NY 11973, USA, and [b]Acquisition Software, Inc., Shoreham, NY 11786, USA. *Correspondence e-mail: ttanabe@bnl.gov

Received 17 February 2017
Accepted 14 June 2017

Edited by M. Eriksson, Lund University, Sweden

Keywords: insertion devices; synchrotron light source; in-vacuum undulator (IVU); storage ring.

The National Synchrotron Light Source (NSLS) ceased operation in September 2014 and was succeeded by NSLS-II. There were four in-vacuum undulators (IVUs) in operation at NSLS. The most recently constructed IVU for NSLS was the mini-gap undulator (MGU-X25, to be renamed IVU18 for NSLS-II), which was constructed in 2006. This device was selected to be reused for the New York Structural Biology Consortium Microdiffraction beamline at NSLS-II. At the time of construction, IVU18 was a state-of-the-art undulator designed to be operated as a cryogenic permanent-magnet undulator. Due to the more stringent field quality and impedance requirements of the NSLS-II ring, the transition region was redesigned. The control system was also updated to NSLS-II specifications. This paper reports the details of the IVU18 refurbishment activities including additional magnetic measurement and tuning.

1. Introduction

In-vacuum undulators (IVUs) have been in operation in various light sources all over the world for more than 30 years. Even though a new generation of more advanced devices such as cryogenic permanent-magnet undulators and superconducting undulators started emerging at some facilities to satisfy special requirements for specific beamlines, IVUs are most often considered as the first choice for short-period undulators due to their commercial availability and ease of operation requiring no cryo-cooling infrastructure and relatively low maintenance costs. IVU18 was constructed by a collaboration of Brookhaven National Laboratory (BNL) and Advanced Design Consulting, Inc. in Ithaca, NY, USA, and was installed in the National Synchrotron Light Source (NSLS) ring in 2006. The New York Structural Biology Center beamline (NYX) decided to reuse this device as a temporary source until funding for a more potent but still experimental source, a segmented adaptive gap undulator (Chubar *et al.*, 2012), becomes available. The NSLS ring was a so-called 'second-generation light source' which mostly relied on bending-magnet radiation. Because of its long electron pulse length and larger emittance, the effect of insertion devices (IDs) on the electron beam at NSLS was not as severe as for the NSLS-II ring. However, the electron beam in the NSLS-II storage ring has a much shorter pulse length and a more tightly focused beam at the source point. Because of this, NSLS-II has much more stringent requirements in terms of field quality and impedance characteristics. Tuning of the magnetic field and implementing less steep transitions at the ends of the device

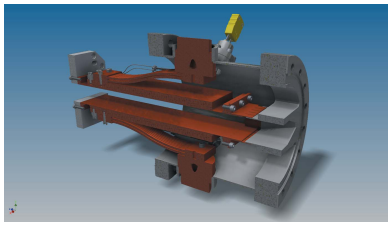

was needed in order for this device to meet these requirements and to reduce the geometric impedance. In §2 a brief description of the IVU18 transition region before the upgrade, requirements for the upgrade, and the design and technical details of the upgraded components are described. This includes descriptions of new vacuum-related components and canting magnets in the straight section. In §3 the upgrade of the control system to the NSLS-II standard motion controller and linear absolute encoder is described. §4 discusses the magnetic field retuning using newly designed and fabricated 'magic finger' modules (Safranek *et al.*, 2002). A vacuum problem which was discovered after installation is discussed in §5. Lastly, a summary is given in §6.

2. Vacuum component update

The original location where IVU18 was installed was very constrained due to the fact that the NSLS ring was not originally designed to accommodate IDs. Hence, the space allocated for the 'tapered transition regions', in which the gap of an IVU gradually changed to a fixed aperture at both ends of the device, were also limited. Fig. 1 shows a cross-sectional view of the original transition region. Flexible thin sheets of Inconel 625 for the variable space were used.

The transverse geometric wake field is given in equation (3.1) of Bane & Krinsky (1993),

$$W_{\perp\mathrm{geo}} = \frac{Z_0\, c}{\pi a}\left(\frac{2\theta}{\pi}\right)^{1/3}\frac{1}{\sqrt{2\pi}\sigma_s}, \qquad (1)$$

where a is the half-gap, σ_s is the bunch length, θ is the tapered angle from the regular chamber to the small gap, and Z_0 = 377 Ω. The impedance requirement of a vacuum transition for the NSLS-II ring has been set to the '10 to 1' rule, namely the slope can change by 1 cm in the transverse direction when the longitudinal dimension changes by 10 cm. The updated design of the region is shown in Fig. 2. It is much simpler than the standard transition design of other NSLS-II IVUs which have flexible water-cooling circuits. This simpler design is possible because the maximum gap for IVU18 is only 20 mm, while

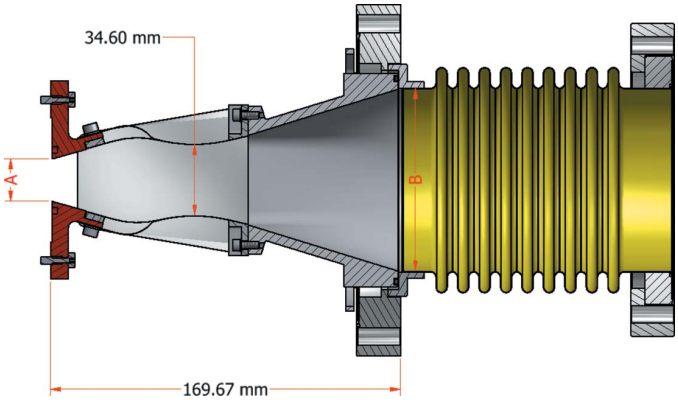

Figure 1
Cross-sectional view of the original taper transition region used at NSLS. Gap A can vary from 5.6 mm to 20 mm while gap B is fixed to 88.5 mm.

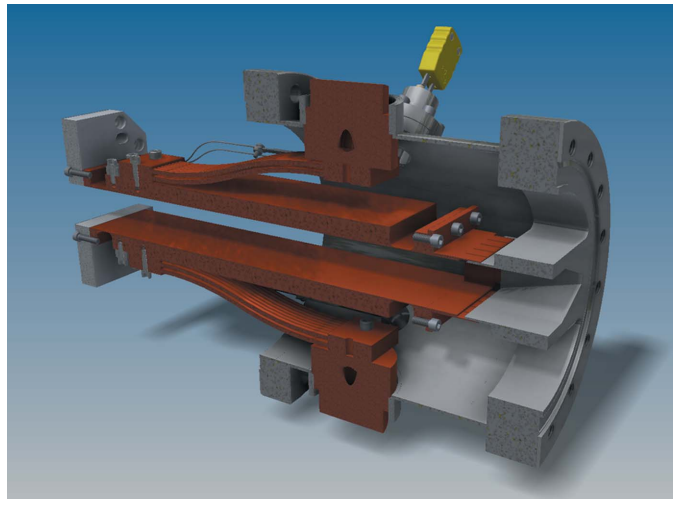

Figure 2
Cutaway view of the newly designed transition region for NSLS-II. Braided flexible thermal straps made of copper are attached to facilitate the transfer of heat from the region close to the magnet arrays. The longitudinal length between flanges is 293 mm.

other IVUs open to 40 mm. Hence, the moving range for IVU18 is more limited and does not require a flexible element. The total length of the region has increased from approximately 170 mm to 293 mm to ensure a more gradual transition than the original design.

Most of the other required vacuum components are mounted onto the front cover of the vacuum chamber for best access. The original configuration included a 500 L s^{-1} combination ion pump/titanium sublimator, a NEG pump (SAES CapaciTorr D1000), an RGA analyzer, a glow discharge cleaning system with associated pumping and view ports, an ion gage, and bleed up ports. This old ion pump was replaced with an NSLS-II 250 L s^{-1} standard ion pump (Gamma Vacuum) and an additional 50 L s^{-1} pump was added to an empty port.

Fig. 3 shows the layout of the straight section with other components such as the electromagnet canting magnets, vacuum pumps and beam position monitors (BPMs). The angle of separation in the canting magnet at the centre is 2 mrad. There is a plan for a second source in the downstream section of the straight for a low-energy anomalous-scattering macromolecular crystallography beamline in the future. ID corrector magnets are of window-frame type and are identical to those used with other IVUs. The canting magnets are also identical to those used in other short straights in the NSLS-II ring.

The original thermal sensors were type-E thermocouples embedded in the magnet platens. Some of these sensors have been damaged and it would have been difficult to replace them without major disassembly. As part of the upgrade, additional PT100 resistance temperature detectors (RTDs) were added for temperature monitoring of the platens. These PT100s are the same Okazaki Ratiopak® mineral insulated resistance thermometer sensors that are used with other IVUs at the NSLS-II facility. One feed-through can accommodate eight

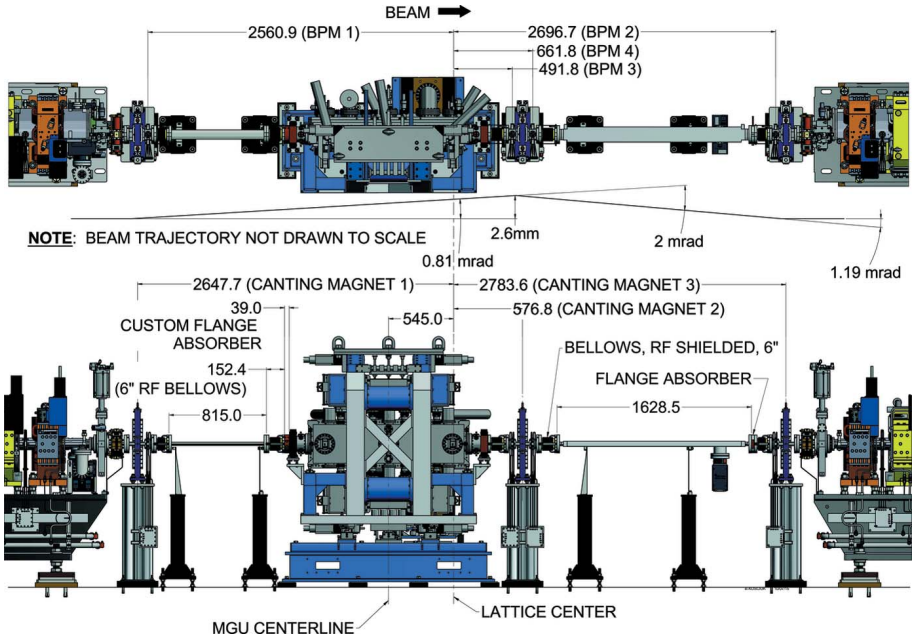

Figure 3
Layout of straight section 19 at NSLS-II.

four-wire RTDs. Two feed-throughs were used and 16 sensors in total were attached to the outer surfaces of magnet arrays. Another modification was the addition of magic finger modules to improve the characteristics of integrated multipoles. The details of the module design and magnetic optimization are discussed in §4.

3. Control system update

The original control system for the device was based on a Parker 6K motion controller and discrete Gemini GT6 micro-stepping drives. Each stepper motor had a shaft-mounted 1000 CPR incremental encoder wired directly to the motion controller and a 24 V DC brake for safety. In addition, each axis also incorporated a Heidenhein absolute linear encoder, an SSI-to-digital converter box and EVM32 input modules to interface the encoder with the parker controller. Heidenhein encoders were used to establish the absolute location of each axis at start-up time, and shaft-mounted incremental encoders were used for closed loop motion control during run time.

The NSLS-II facility standardized ID motion controls and selected a Delta Tau Turbo PMAC2 motion controller as the standard platform. In order for the undulator to be compatible with the new standard, a major update of the control system was required. To expedite development and reduce upgrade costs, existing Parker stepper motors on the device and their associated amplifiers from the original system were reused. NSLS-II also standardized the use of Renishaw RESOLUTE^{TM} absolute linear encoders for IDs, and the NYX undulator was retrofitted with 5 nm-resolution Renishaw encoders on each axis. These encoders are BiSS-C interface devices and fully compatible with Delta Tau motion controllers. Fig. 4 shows a block diagram of the updated control system. The Delta Tau controller was set up to provide step and direction signals to the GT6 stepper drives, and a dual feedback PID loop was set up which utilized absolute linear encoders for position feedback and shaft-mounted incremental encoders for velocity feedback. Undulator motors were configured in the control software to use the PMAC standard coordinate system and achieve a standardized motion control interface with Experimental Physics and Industrial Control System (EPICS) PMAC support libraries (http://www.aps.anl.gov/epics/).

A Linux (Debian 7) based host computer functions as the EPICS IOC server for the undulator device and communicates with the Delta Tau Brick Controller through an Ethernet TCP/IP interface. The IOC server provides access to desired

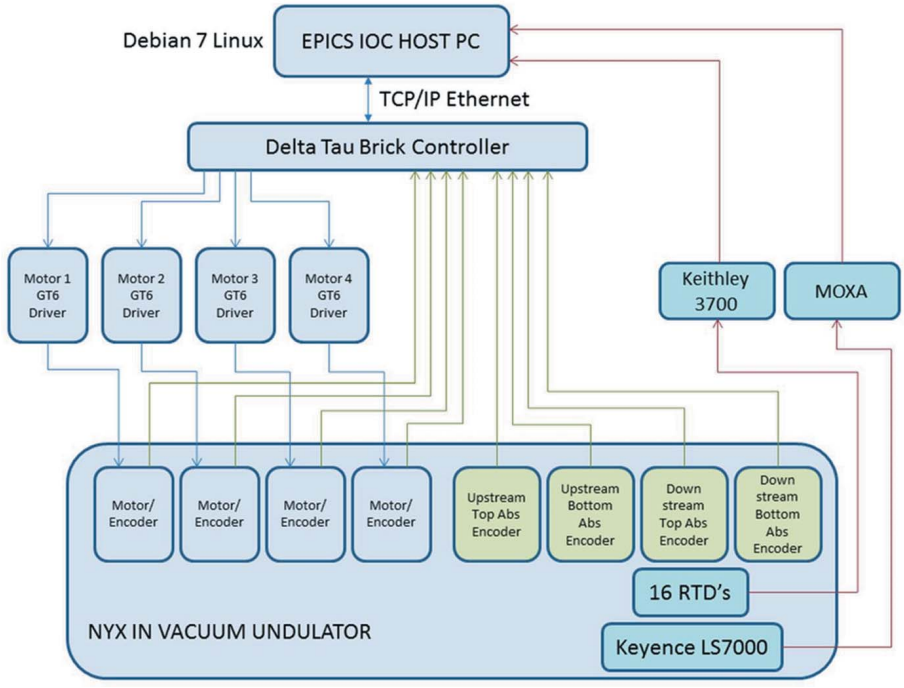

Figure 4
Block diagram of the updated control system design.

process variables on the undulator and facilitates control and monitoring of various functions. A Control System Studio (http://controlsystemstudio.org/) based BOY graphical user interface screen was develop as the front-end operational control screen for the new control system as shown in Fig. 5. The screen provides users with the ability to control the desired gap and has various indicators that show the status of various hardware on the undulator (limit switches, RTD temperature, *etc.*). Any controller faults are also reported to the user through the same screen. An engineering mode screen provides the user with low-level control of each motor and has buttons that can be used to clear any system faults. A Keyence LS7501 optical sensor on the existing device was reused to monitor the undulator gaps *in situ*. The Keyence system is used for monitoring purposes only and does not feed back into the motion control system. New software to monitor gap readings through an RS-232 serial communication port on the Keyence controller was developed as part of the control system update.

Table 1
NYX-IVU specifications.

Item	Parameter
Magnet core length	>1.0 m
Period length	18 mm
Minimum operational magnetic gap (mingap)	5.6 mm
Nominal peak By at 5.6 mm gap	0.95 T
$K_{\rm eff}$ at 5.0 mm gap	>1.81
Gap scanning requirement	30 eV s^{-1} or greater, over usable photon energy range
First and second integral error requirement ($\|x\|$ < 10 mm, $\|y\|$ = 0 mm), (mingap ≤ gap ≤ maxgap)	
$\int_{-\infty}^{\infty} By(x, y, z)\,dz$ (absolute value without correction coils)	<50 G cm
$\int_{-\infty}^{\infty} Bx(x, y, z)\,dz$ (absolute value without correction coils)	<30 G cm
$\int_{-\infty}^{\infty}\int_{-\infty}^{z} By(x, y, z')\,dz'\,dz$ (absolute value without correction coils)	<5000 G cm cm
$\int_{-\infty}^{\infty}\int_{-\infty}^{z} Bx(x, y, z')\,dz'\,dz$ (absolute value without correction coils)	<2000 G cm cm
On-axis electron trajectory requirements for E = 3 GeV at any longitudinal position	$\|x\|$ < 5.0 µm, $\|y\|$ < 2.0 µm and $\|y'\|$ < 10 µrad
Integrated multipole requirement ($\|x\|$ < 10 mm, y = 0 mm), (mingap ≤ gap ≤ maxgap)	Definition of multipole expansion about ($x = x_0$, y = 0)† $\int_{-\infty}^{\infty} dz(B_y + iB_x) = \sum_{n=0}^{\infty}[b_n(x_0) + ia_n(x_0)](x - x_0 + iy)^n$
Normal quadrupole [$\|b1(x0)\|$]	50 G
Skew quadrupole [$\|a1(x0)\|$]	50 G
Normal sextupole [$\|b2(x0)\|$]	50 G cm^{-1}
Skew sextupole [$\|a2(x0)\|$]	50 G cm^{-1}

† The reference points (x_0, 0) should be chosen less than 2.5 mm apart, *e.g.* x_0 = −6 mm, −4 mm, −2 mm, 0 mm, 2 mm, 4 mm, 6 mm.

4. Magnetic measurement and additional field tuning

Table 1 shows the required specifications for NSLS-II operation. For comparison purposes, the ID magnetic field specifications at the NSLS are shown in Table 2.

We re-measured the device at the state-of-the-art NSLS-II magnetic measurement facility (Musardo *et al.*, 2013). It was shown that the normal sextupole was more than four times larger than the NSLS-II requirement. At the time when this device was built at the NSLS, there was only a Hall probe bench and pulsed wire bench. Our multipole measurement was based on a Hall probe measurement and its repeatability was only ±10 G cm. In addition, the multipole fitting was performed with a wider horizontal area than it should have been. Some of the increase in the sextupole components could be attributed to the degradation of magnet arrays but it is fair to say that such large sextuple components were smeared out by the original measurement and were not detected. Fig. 6 shows the ratio of the peak fields measured in 2006 to those in 2015.

Table 2
NSLS insertion devices specifications.

Normal/skew dipole	100 G cm
Normal/skew quadrupole	10 G / 100 G
Normal/skew sextupole	50 G cm^{-1}
Normal second integral	80000 G cm
Skew second integral	80000 G cm
RMS phase shake	2°

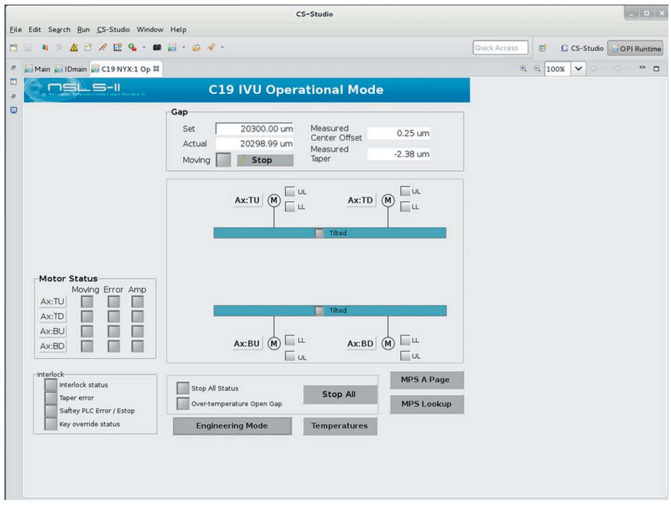

Figure 5
Control System Studio BOY based operation screen for the undulator.

A new measurement shows that the first several periods and the last few periods were demagnetized. A difference in the baseline of approximately 1% may be attributed to calibration errors in the old measurement system. Calculations of the multi-electron emission-based on-axis flux at a gap of 6 mm for both the 2006 and 2015 data are shown in Fig. 7. Electron beam parameters used for these calculations can be found on the official BNL web page (NSLS-II, 2017). The RMS phase error has deteriorated from 1.85° to 2.35°. However, no appreciable flux reduction is observed about the fifth harmonic despite the demagnetization. The blue-shifted

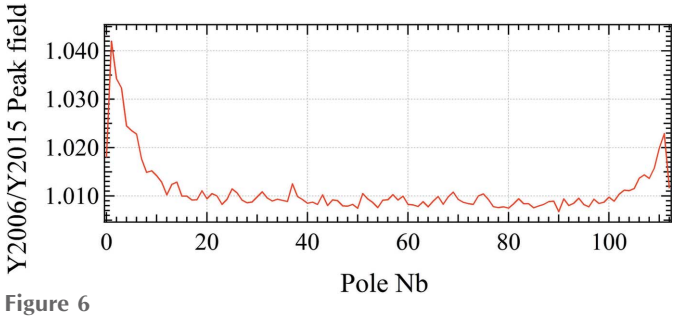

Figure 6
Ratio of peak fields at 5.6 mm gap measured in 2006 to those measured in 2015. The maximum decrease of the peak field is approximately 3% at the entrance of the device and 1% at the exit.

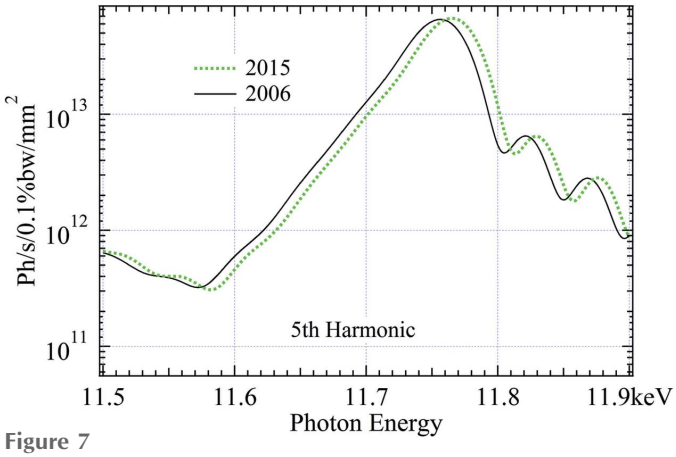

Figure 7
Comparison of fluxes from the measurement data taken in 2006 and 2015. Shown is the fifth harmonic radiation at a gap of 6.0 mm.

spectrum is due to an average 1% reduction of the field for the 2015 measurement as compared with the 2006 measurement.

The field quality of the original MGU-X25 was tuned with wire and steel shims (Tanabe *et al.*, 2007). New magic finger modules have been designed to optimize integrated multipoles for this device. Pill magnets 2 mm in diameter and 4 mm in height with a remanent field of 1.2 T having a titanium nitride coating were used. Two rows of staggered holes ensure a 1.75 mm spacing between holes for smooth tuning. The first row has 15 holes and the second row 14. The optimization of the magic finger pill magnet placement was carried out using *IDBuilder*, a genetic algorithm-based computer code for magnetic tuning of undulators (Chubar *et al.*, 2007). Fig. 8 shows a simplified drawing of the magic finger unit used for this device.

Figs. 9(*a*) and 9(*b*) show the results of horizontal and vertical field integral measurements and predictions by the *IDBuilder* software. Table 3 shows the results of the measurement for multipoles before and after magic finger correction.

5. Vacuum issues after installation

Vacuum leak tests were conducted after pre-baking the device in the Insertion Device Magnetic Measurement Facility (IDMMF). The device was found to be leak tight at that time. However, after installation and *in situ* baking in the ring, a small leak was detected. It was found that there was a non-negligible leak from the insulating vacuum, which was originally intended for cryo-gas operation, to the main vacuum. After a multi-stage roots pump with a gas ballast was attached to the insulating vacuum section, the vacuum level in the IVU chamber stayed below the 10^{-9} torr required for operation. However, there appeared to be evidence of an argon instability which is shown in Fig. 10. After disassembly *in situ*, a temporary fix was applied to seal the insulating vacuum pipe. During the December 2016 shutdown, one water feed-through which was found to be leaking was removed and closed off. After this operation, there was no more evidence of an argon instability.

Table 3
Integrated multipole values before/after magic finger (MF) correction.

	Normal/skew dipole (G cm)	Normal/skew quadrupole (G)	Normal/skew sextupole (G cm^{-1})
Before MF correction	−5.4/−125	68.0/82.5	237.6/64.5
After MF correction	0.95/−12.1	1.39/−13.6	39.6/17.2

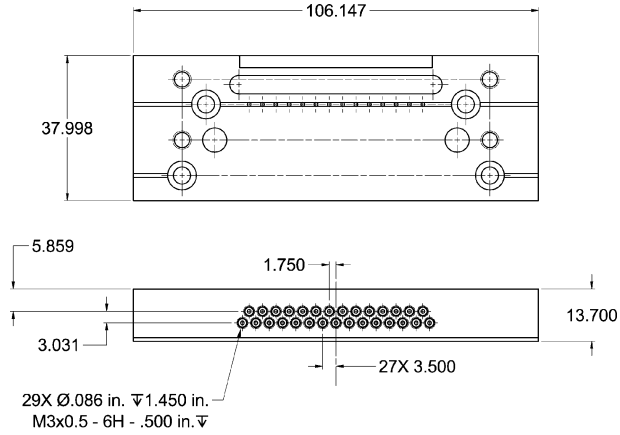

Figure 8
Part of the magic finger drawing showing the magnet hole patterns. All dimensions are in millimeters.

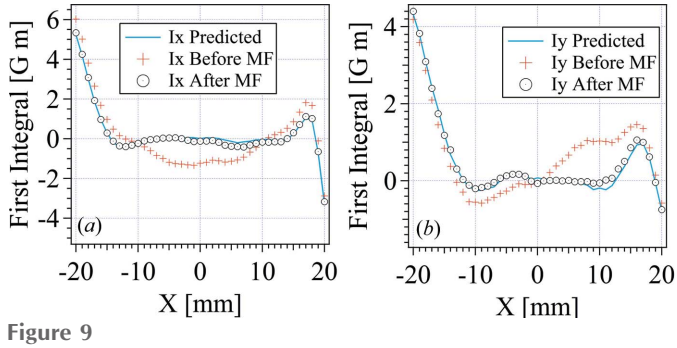

Figure 9
Comparison between the measured horizontal (*a*) and vertical (*b*) field integrals before and after magic finger (MF) corrections, and the *IDBuilder* predictions.

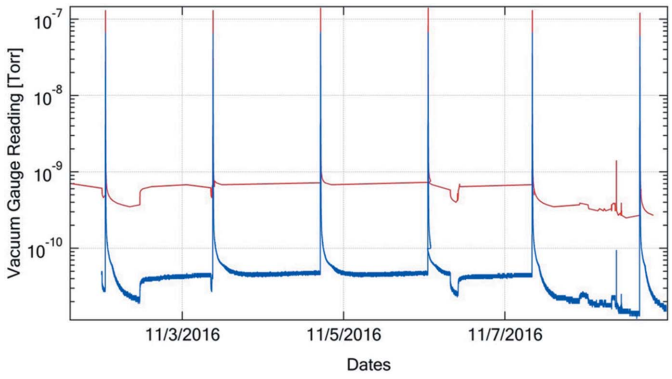

Figure 10
Indication of noble gas instability shown in the readings of a cold cathode gauge (red) attached in the vacuum chamber of the device and those of a vacuum gauge installed in an ion pump also attached to the chamber.

6. Conclusion

An IVU used for nine years in the NSLS ring has been modified to be utilized in the NSLS-II ring. Extensive modifications on the design of the transition regions, control system and temperature monitoring have been carried out. Multipole field retuning was carried out using *IDBuilder*, originally developed for the SOLEIL synchrotron in France. The beamline was commissioned without any issues in a few days. A small leak from the insulating vacuum to the ring vacuum was temporarily repaired during the December 2016 shutdown. A fundamental reconfiguration of the cooling system is planned for 2017.

Acknowledgements

The authors thank technicians of the NSLS-II ID group and Vacuum group for their dedication and hard work under an extremely tight schedule. This manuscript has been authored by employees of Brookhaven Science Associates, LLC, under Contract No. DE-SC0012704 with the US Department of Energy.

References

Bane, K. & Krinsky, S. (1993). BNL Informal Report BNL-48792. Brookhaven National Laboratory, Brookhaven, NY, USA.
Chubar, O., Bengtsson, J. A., Blednykh, A., Kitegi, C., Rakowsky, G. & Tanabe, T. (2012). *Proceedings of the Third International Particle Accelerator Conference (IPAC12)*, New Orleans, LA, USA, p. 766.
Chubar, O., Rudenko, O., Benabderrahmane, C., Marcouille, O., Filhol, J. M. & Couprie, M. E. (2007). *AIP Conf. Proc.* **879**, 359–362.
Musardo, M., Kitegi, C., Rakowsky, G., He, P., Rank, J., Cappadoro, P., Fernandes, H., Harder, D. A., Corwin, T., Licciardi, W. & Tanabe, T. (2013). *Proceedings of the 25th North American Particle Accelerator Conference (NA-PAC'13)*, 29 September–4 October 2013, Pasadena, CA, USA, p. 1172.
NSLS-II (2017). *NSLS-II Storage Ring Parameters*, https://www.bnl.gov/ps/accelerator/.
Safranek, J., Limborg, C., Terebilo, A., Blomqvist, K. I., Elleaume, P. & Nosochkov, Y. (2002). *Phys. Rev. ST Accel. Beams*, **5**, 010701.
Tanabe, T., Ablett, J., Berman, L., Harder, D. A., Hulbert, S., Lehecka, M., Rakowsky, G., Skaritka, J., Deyhim, A., Johnson, E., Kulesza, J. & Waterman, D. (2007). *AIP Conf. Proc.* **879**, 283–286.